Environ Sci Pollut Res (2015) 22:870–881
DOI 10.1007/s11356-014-2973-x

Fenton-like processes and adsorption using iron oxide-pillared clay with magnetic properties for organic compound mitigation

Aline Auxiliadora Tireli · Iara do Rosário Guimarães · Júlio César de Souza Terra · Robson Rosa da Silva · Mário Cesar Guerreiro

Received: 21 November 2013 / Accepted: 23 April 2014 / Published online: 10 May 2014

Abstract In this work, a new step was added to the classic route of iron-pillared clay obtention, resulting in a material with both magnetic and oxidative properties. The saturation of the material surface intercalated with trinuclear acetate-hydroxo iron (III) nitrate in glacial acetic acid atmosphere before heat treatment promoted magnetic phase formation (FePMAG). The material was characterized by Fourier transform infrared spectroscopy (FTIR), X-ray diffraction (XRD), nitrogen adsorption/desorption isotherms, scanning electron microscopy coupled with energy dispersive spectroscopy (SEM/EDS), and X-ray photoelectron spectroscopy (XPS). FePMAG showed an increase of 0.57 nm in basal spacing which contributed to the specific surface area increase from 39.1 to 139.2 m^2/g. The iron phase identified by XRD and XPS was maghemite, with a little presence of hematite formed by the trinuclear acetate-hydroxo iron (III) nitrate decomposition during heat treatment. In the adsorption tests, FePMAG displayed a good capacity for organic dye methylene blue (MB) removal, reaching 41 % at 150 min. Under photo-Fenton conditions, the material showed an excellent MB oxidation capacity, completely removing the color of the solution within 90 min. Identification of the oxidation products with lower molecular (m/z=160, 220, and 369) mass was performed by electrospray ionization mass spectroscopy (ESI-MS).

Keywords Pillared clay · Organic compound · Photo-Fenton · Oxidation mechanism

Introduction

Textile production results in high levels of pollution due to the great volume of dyes disposed in effluents. Dyes are a serious problem when dealing with textile waste because they are water-soluble and chemically and photolytically stable (Guimarães et al. 2012). Methods that can contribute to the removal of these molecules in aqueous media are extensively studied, since dyes can be environmentally problematic (Papic et al. 2009), carcinogenic, mutagenic, and toxic (Banković et al. 2012). Effluents containing dyes cannot be disposed in natural waters, since even small amounts of those are able to reduce the solar light penetration and decrease the dissolved oxygen quantity, damaging aerobic processes (Banković et al. 2012; Bergamini et al. 2009).

Advanced oxidation processes (AOP) have been extensively used in the treatment of wastewater from the textile industry, as it has been seen that dye degradation and removal is very hard to be carried out (Galeanoa et al. 2010; Guimarães et al. 2012; Homlok et al. 2013; Zhiyong et al. 2013) when conventional treatments are employed. In a process of photocatalytic oxidation, the initial step consists in the adsorption of the substrate on the photoactive support, which is according Damardji et al. (2009) the fundamental photocatalytic degradation mechanism. The second step is the photoreaction between the adsorbed substrate and the support, by formation of *electron-hole* pairs in the conduction and valence bands. Thus, the material offering the best combination of properties such as adsorption and photo-activity will have a higher efficiency for mineralization of pollutants.

Responsible editor: Philippe Garrigues

A. A. Tireli (✉) · I. R. Guimarães · J. C. S. Terra · M. C. Guerreiro
Department of Chemistry, Federal University of Lavras, Lavras, MG 37200-000, Brazil
e-mail: aatireli@gmail.com

R. R. da Silva
Institute of Chemistry, São Paulo State University, Araraquara, SP 14801-970, Brazil

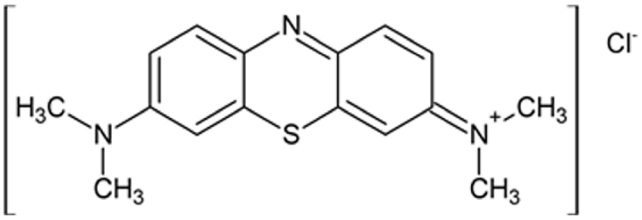

Fig. 1 Representative structure of the organic dye methylene blue (MM=284 g mol^{-1})

In this context, one of the main goals of the academic community has been the finding of new synthetic routes for materials with developed surface area, small particle size, and high photo-activity. Among several proposed materials, pillared clay (PILC) has received considerable attention due to the possibility of using semiconductor pillars for the synthesis of materials with combined functionality. The photocatalytic activity of clay with titanium oxide pillars is much greater than that observed for pure oxide (Fatimah et al. 2010).

The pillaring process consists of the following three-step synthesis procedure: (i) polymerization of a multivalent cation (polycations), (ii) intercalation of the polycation in the interlayer space of the clay, and (iii) controlled heat treatment (Gil et al. 2011). The latter step transforms the polycations into stable oxi-hydroxide phases named *pillars* that contribute to sustain the layered structure of the clays. The pillaring promotes increased basal spacing and surface area, which provides better accessibility of the molecules to the active sites present inside the clay structure (Bergaya et al. 2006; Gil et al. 2011; Yang et al. 2013).

Magnetic materials became very interesting and economically viable because they allow easier and more convenient processes for isolation of the catalyst and recycling (Ferroudj et al. 2013; Garrido et al. 2010; Zhenyan et al. 2011) and have also been reported for the removal of waste dyes in effluents (Ebner et al. 2001; Tuutijärvi et al. 2009; Yu and Yang 2010).

This study, therefore, aims to synthesize a new material with photocatalytic properties and that may be applied in the degradation of organic dyes. The material was obtained by a simple and inexpensive method, with the addition of a step to the traditional pillaring process. The result was a material with both magnetic and semiconductor properties combined.

Experimental

Catalyst preparation

Montmorillonite clay (San Luís, Argentina) with cation exchange capacity (CEC) of 175 mmol/100 g of clay was used in this work. Before use, Na^+ was inserted into the clay structure (Khalaf et al. 1997) to facilitate the subsequent exchange with the oligomer, with Na^+ now being the principal exchangeable cation of montmorillonite. The oligomer trinuclear acetate-hydroxo iron (III) nitrate was obtained by the method described by Yamanaka et al. (1984). A 0.04-mol-dm^{-3} solution of this oligomer was intercalated to montmorillonite suspension under vigorous stirring. The intercalated material

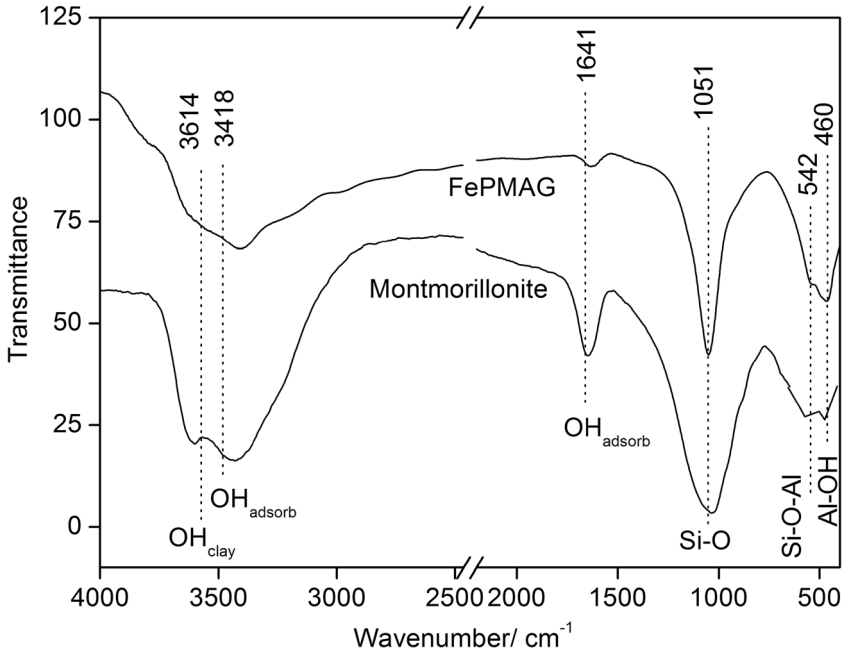

Fig. 2 FTIR spectra of the FePMAG and montmorillonite

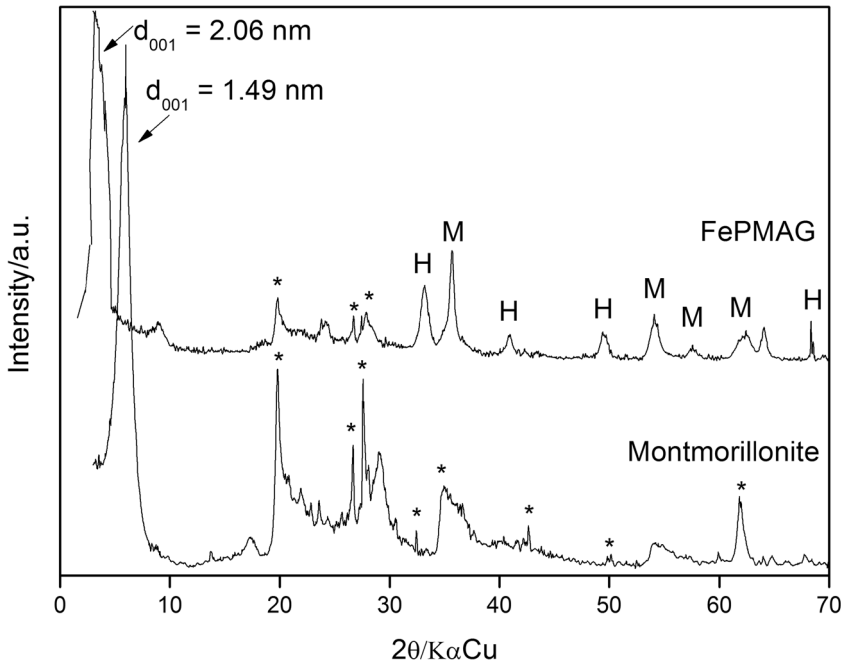

Fig. 3 Diffraction profiles obtained for FePMAG and montmorillonite (* = montmorillonite, M = maghemite, and H = hematite)

was separated by centrifugation and washed several times with water for NO_3^- and Na^+ removal.

Preceding the heat treatment, the intercalated material was stored in an acetic acid atmosphere at room temperature (25.0 ±1.0 °C) for 72 h. This step was added to the synthesis in this work, in order to achieve magnetic iron phases during heat treatment. Then, the intercalated material was submitted to controlled heating in atmospheric air from 25 to 500 °C at a heating rate of 10 °C/min. The material remained at 500 °C for 1 h. The resulting material was named FePMAG.

Catalyst characterization

Fourier transform infrared spectroscopy (FTIR) spectra were recorded on a Digilab Excalibur spectrometer with a spectral range from 400 to 4,000 cm^{-1}. Samples were ground to a powder and pressed into KBr pellets. The FTIR spectra with a resolution of 4 cm^{-1} were collected over an average of 32 scans. XRD analyses were performed on a Rigaku (Japan) D/Max 2500 VB2+/PC X-ray powder diffractometer operating with Kα radiation of Cu (λ=0.15406 nm), a generator voltage of 45 kV, and a current of 30 mA in 2θ ranging from 2° to 60°. Nitrogen adsorption/desorption isotherms were obtained with an Autosorb1mp, Quantachrome. The specific surface area was calculated using the BET model. The total pore volume was estimated from the amount of nitrogen adsorbed at P/P_0=0.995, and the pore size distribution was calculated based on the DFT equation. All samples were degassed overnight at 300 °C before each adsorption measurement. Scanning electron microscopy (JEOL Ltd.) was coupled with an energy dispersive X-ray analyzer (INCA 350, Oxford Instruments). X-ray photoelectron spectroscopy (XPS) measurements were carried out using an AEI ES200B spectrometer with a base pressure smaller than 10^{-9} Torr using MgKa X-ray radiation (hν=1,253.6 eV). Spectra were recorded to achieve maximum instrument resolution (better than 0.8 eV). Binding energies were calibrated using O 1 s from oxide in the samples taken as 529.9 eV.

Methylene blue adsorption and oxidation tests

The organic dye methylene blue (Fig. 1) was employed in both adsorption and oxidation (Fenton and photo-Fenton) tests. Kinetic assays were conducted in defined intervals (15, 30, 60, 90, 120, and 150 min) for (i) adsorption, (ii) Fenton-like (FePMAG+H_2O_2), and (iii) photo-Fenton (λ=254 nm+FePMAG+H_2O_2), and all the experiments were carried out in 80 mL of 50 mg/L MB solutions and 30 mg of FePMAG. Samples were taken from the reaction in the defined intervals and centrifuged, and the remaining concentration was determined by UV-Vis spectroscopy (665 nm) (Shimadzu UV1800). Scans were also performed from the ultraviolet to visible (200 to 800 nm) for all reaction times. After the reactions, the catalyst was removed from the reaction medium by attraction using a permanent magnet.

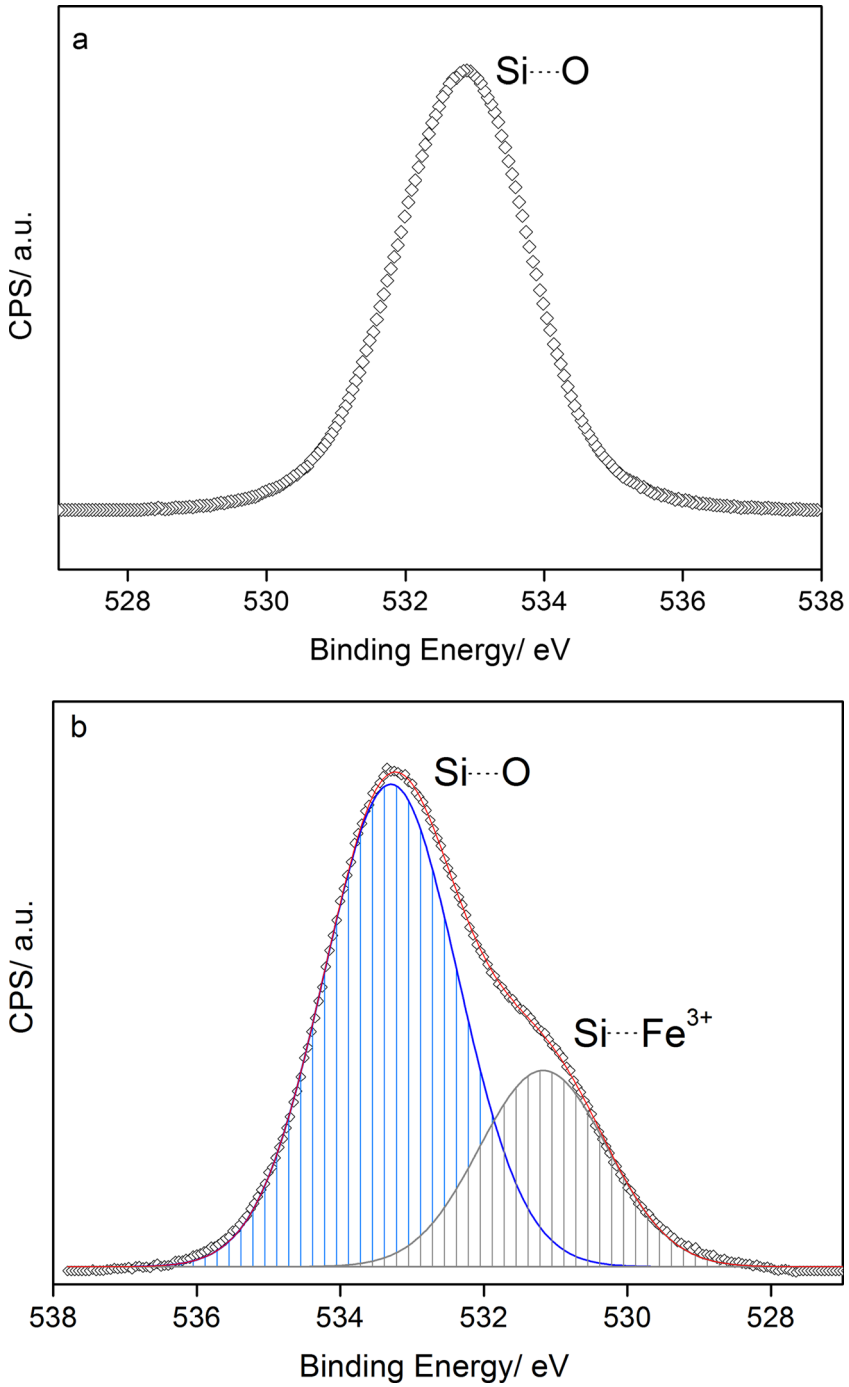

Fig. 4 O 1 s XPS spectra of **a** montmorillonite and **b** FePMAG

Oxidation studies via electrospray ionization mass spectroscopy

The experiments using mass spectrometry with electrospray ionization (ESI-MS) were performed in Agilent 1100 Series LC/MSD trap equipment in positive ion mode to identify the intermediate chemical species of methylene blue oxidation reaction. Spectra were obtained by 50 scans of 0.2 s each. The analysis conditions were as follows: heat capillary temperature 350 °C, dry gas flow 5 L min^{-1}, pressure 15 psi, and capillary voltage −3.5 kV.

Results

Characterizations

The saturation of the FePMAG surface with acetic acid was performed in order to obtain, in the end, a material with

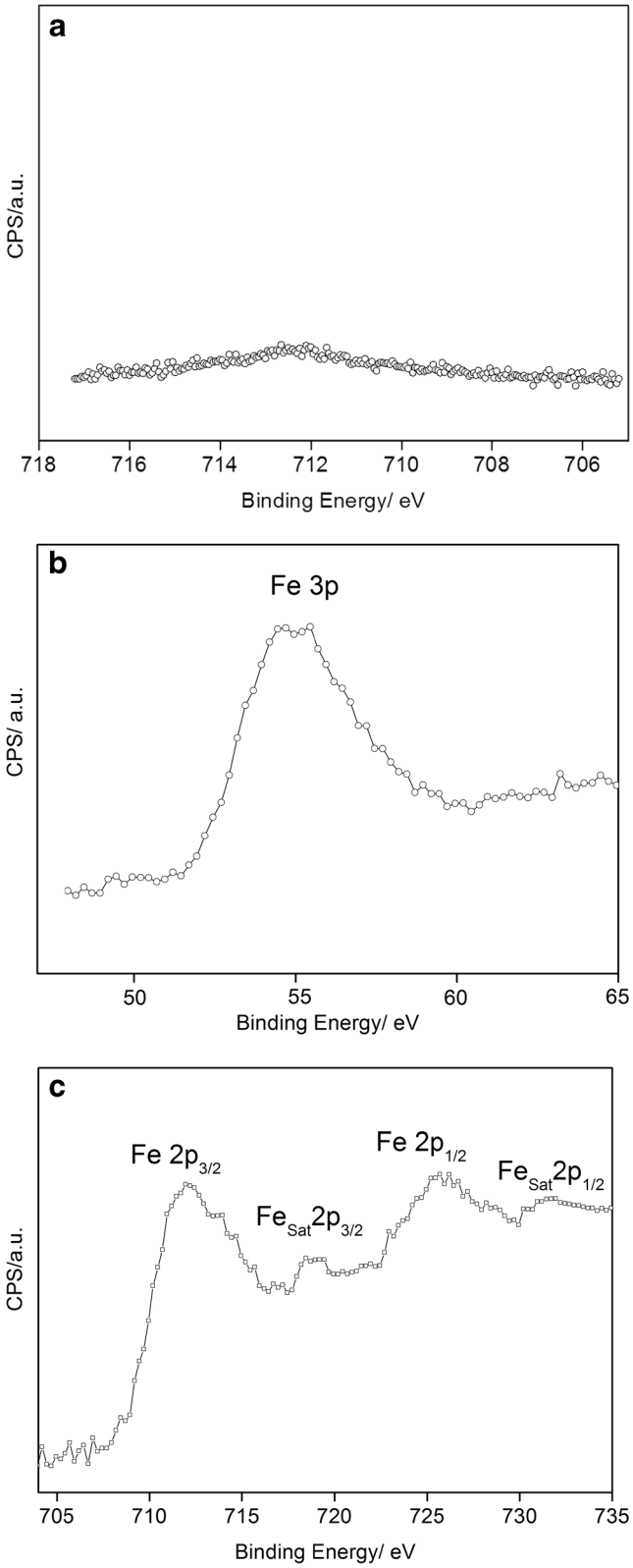

Fig. 5 XPS spectra of **a** Fe 2p montmorillonite, **b** Fe 3p FePMAG, and **c** Fe 2p FePMAG

magnetic properties, which facilitates the isolation and recycling of the catalyst when the reaction is over (Pan et al. 2011). Yu and Yang (2010) developed a similar synthetic route for magnetic clay obtention, and these authors exposed the material intercalated with $FeCl_3 \cdot 6H_2O$ to acetic acid steam at 80 °C during 2 h.

The spectra in the infrared region (Fig. 2) showed a strong reduction in the intensity of bands at 3,600 and 3,400 cm^{-1} relative to OH stretching of the constituent of the octahedral sheet and adsorbed water on the clay surface, respectively (Nogueira et al. 2009). The 3,400 band reduction after heat treatment is expected due to the release of water molecules. At 1,641 cm^{-1}, the band refers to OH vibration of adsorbed H_2O, the one at 1,051 cm^{-1} is related to Si-O stretches, and finally, two deformation vibrations at 542 and 460 cm^{-1} refer to Si-O-Al and Al-OH, respectively (Tyagi et al. 2006). The intensity of the latter two bands is higher for FePMAG, which can be attributed to overlapping with two hematite characteristic bands around 550 and 460 cm^{-1} (Cai et al. 2014).

The diffraction profiles of both FePMAG and montmorillonite are shown in Fig. 3. For the montmorillonite, a typical pattern was observed, with an intense 2θ=6.04 reflection relative to the basal spacing d_{001} (1.498 nm). The other reflections are corresponding to montmorillonite's crystalline structure (2θ=19.82°, 26.65°, 27.65°, 32.47°, 34.90°, 50.16°, and 61.92°) (Alvarez-Puebla et al. 2004; Ayodele et al. 2012).

The modified clay FePMAG showed a diffraction profile with reduction on the reflections related to the associated minerals. The great reflection observed in 2θ=3.24 is related to basal spacing d_{001} (2.064 nm), confirming the success of the pillaring process. Other diffractions are related to the presence of hematite (2θ=33.22°, 40.93°, 49.40°, and 68.36°) and maghemite (2θ=35.75°, 54.08°, 57.49°, and 62.30°) iron phases, also reported by Afkhami et al. (2010), Jung et al. (2012), and Yu and Yang (2010), which are formed with degradation of the trinuclear acetate-hydroxo iron (III) during heat treatment. But since the XRD patterns of γ-Fe_2O_3 and Fe_3O_4 are very similar, it is difficult to distinguish the two phases simply from the XRD patterns (Tuutijärvi et al. 2009). The formation of a magnetic iron phase is indicated by the material's attraction for a permanent magnet, so XPS was used in order to distinguish the two different possible phases.

The O 1 s spectra for both the montmorillonite and FePMAG are shown in Fig. 4a, b. In the montmorillonite profile, the single peak fitted in 533.1 eV occurs due to Si-O interaction, which is expected because of the fact that in a 2:1 montmorillonite, the surface is formed by silicon and oxygen tetrahedrons. For FePMAG, the signal related to Si-O shifting to 531.6 eV presented a small shoulder due to the strong interaction between Si-O (clay structure) and Fe^{3+} (iron oxides) (Coelho et al. 2014), indicating that a portion of the iron inserted into the clay structure is deposited on the surface, interacting with the tetrahedral sheets of the clay, without destroying the original framework.

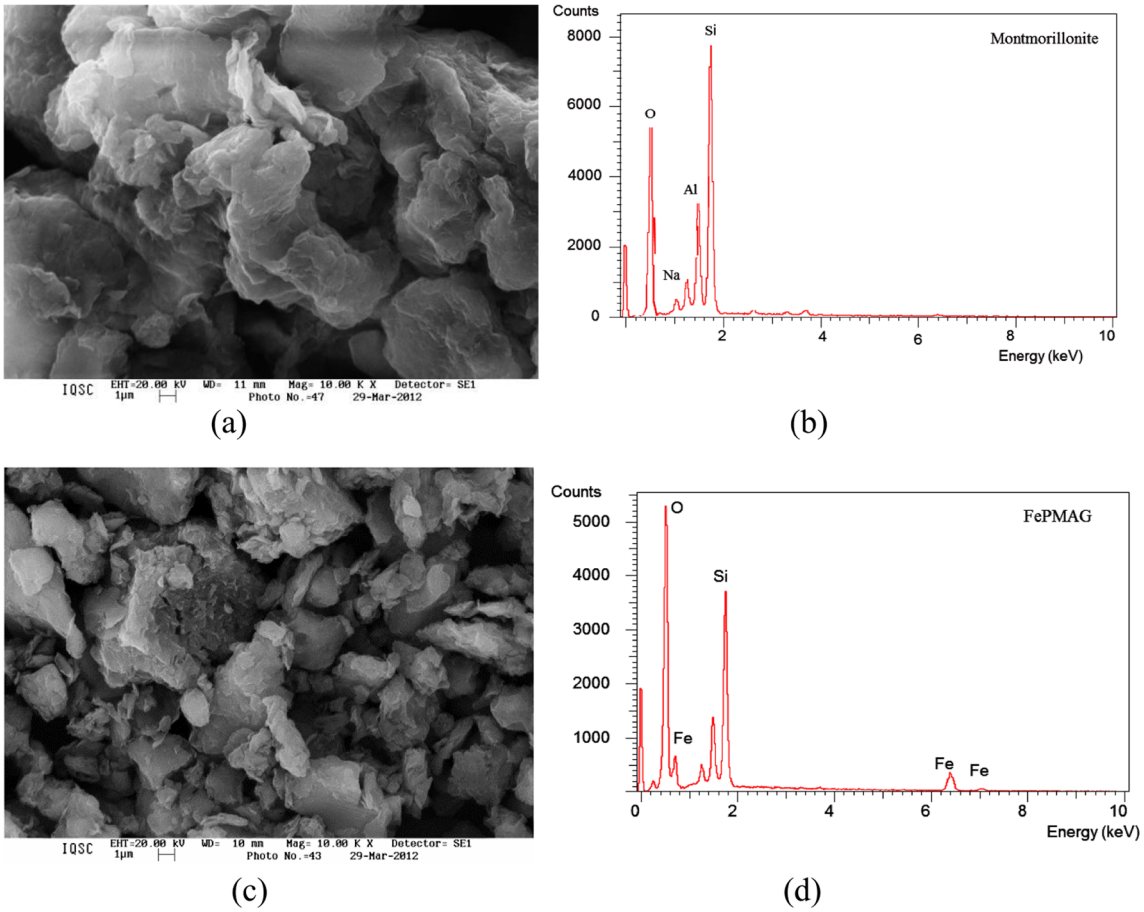

Fig. 6 Scanning electron microscopy (SEM) coupled with energy dispersive spectroscopy (EDS) patterns for montmorillonite (**a**, **b**) and FePMAG (**c**, **d**)

As expected, the XPS Fe 2p montmorillonite's spectrum did not show any signal, indicating the absence of iron on the surface of the material (Fig. 5a). The Fe 2p spectrum for FePMAG provides very complex data with the presence of peaks centered around 712 and 725 eV corresponding to Fe $2p_{3/2}$ and Fe $2p_{1/2}$ regions (Fig. 5c), besides the presence of satellites around 718 and 731 eV, which characterize the γ-Fe_2O_3 oxide phase (Aronneiemi et al. 2004; Coelho et al. 2014; Wang et al. 2013). The peak observed around 712 eV is not entirely uniform, showing a shoulder near 714 eV; this overlapping peak was similarly mentioned in a previous work and corresponded to the presence of a portion of iron in the α-Fe_2O_3 phase (Aronneiemi et al. 2004). The Fe 3p XPS spectrum is presented in Fig. 5b, and a single peak centered in 55 eV is characteristic of maghemite iron oxide, as reported by Liu et al. (2006) and Yamashita and Hayes (2008).

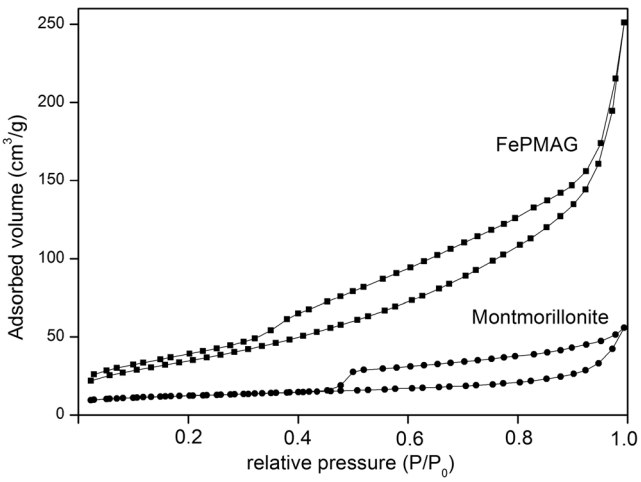

Fig. 7 Nitrogen adsorption/desorption isotherms at 77 K for montmorillonite and FePMAG

Table 1 BET area, pore size, and volume for the samples

Sample	d_{001}	S_{BET} (m^2/g)	V_{total} (cm^3/g)	Pore size (nm)
FePMAG	2.06	139.2	0.386	1.49
Montmorillonite	1.49	39.1	0.066	3.20

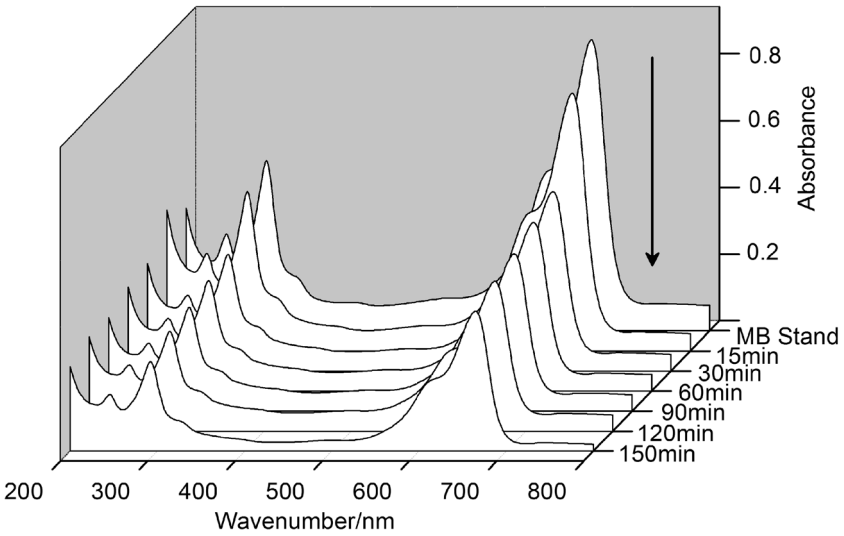

Fig. 8 Kinetic study of the adsorption of methylene blue with FePMAG (conditions: [MB]= 50 mg/L; V_{MB}=80 mL; m_{FePMAG}=30 mg; T=25±1 °C; pH=6)

Scanning electron microscopy (SEM) coupled with energy dispersive spectroscopy (EDS) provides a semiquantitative elemental analysis of the material surface. For the montmorillonite (Fig. 6b), Si, Al, O, and Na are the constituents of the clay structure, with Si, Al, and O being the major elements. Since the structure of the material consists of Si-O tetrahedron and Al-O octahedron, the data profile is consistent with the expected; furthermore, after the change mentioned in the "Experimental" section, Na is the main exchangeable cation. FePMAG showed a significant decrease in Na amounts, corroborating with the expected in the pillaring process, once Na^+ is replaced by trinuclear acetate-hydroxo iron (III).

EDS analysis indicates an increase in the amount of iron on the surface of FePMAG. This corroborates with the XPS results, indicating that iron not only entered the clay layers, but also a portion of it was deposited out of the layer. That change in the amount of iron on the surface of the material leads to a substantial increase in the adsorption and/or catalysis activity due to changes in the structure of surface sites available for the reaction to take place (Brillas et al. 2009).

The increase in both specific surface area and total pore volume is an important factor to confirm the success of the pillaring process (Banković et al. 2012). In this work, the pillaring process was confirmed again by the significant increase of the surface area by a factor of about 3.5. This value is very significant when it comes to iron-pillared clays, and other authors have reported 36.8 m^2/g (Hou et al. 2010) and 108 m^2/g (Caudo et al. 2007).

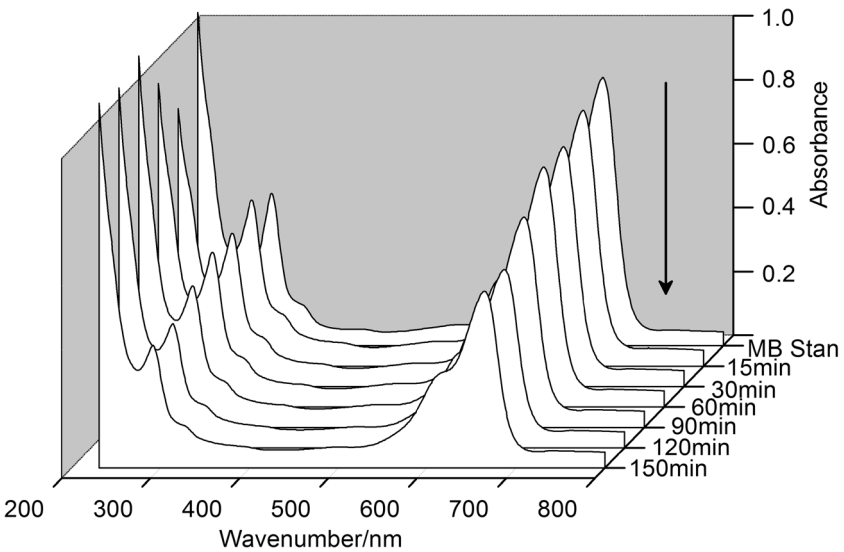

Fig. 9 Kinetic study of methylene blue oxidation with FePMAG via the Fenton-like process (conditions: [MB]= 50 mg/L; V_{MB}=80 mL; m_{FePMAG}=30 mg; [H_2O_2]= 0.03 mol dm^{-3}; T=25±1 °C; pH=6)

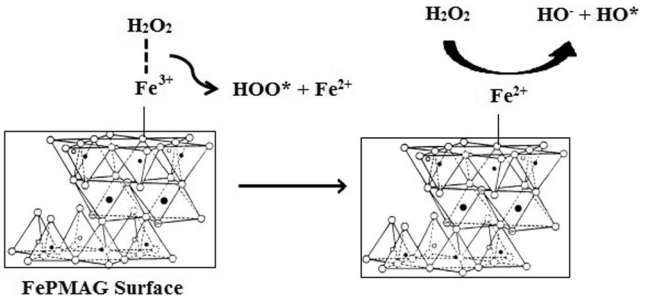

Fig. 10 Fenton-like process in Fe^{3+} surface

The isotherms (Fig. 7) were categorized as type II and, for all materials, hysteresis loop 3 typical of aggregated powders such as clays (Letaief et al. 2003; Rouquerol et al. 1999). The specific surface area and total pore volume for the FePMAG and the natural clay are shown in Table 1, and these corroborate with the increase in the basal spacing found in the XRD analysis.

Methylene blue adsorption and oxidation tests

After the successful pillaring process, with a new material having a higher surface area and iron pillars not only inside the structure but also dispersed on the surface, the clay FePMAG was evaluated on its methylene blue (MB) adsorption and oxidation (Fenton-like and photo-Fenton) capacities (Fig. 1).

The results found in the adsorption tests in defined time intervals (15 and 150 min) are shown in Fig. 8, and the decoloration of the solution was determined by UV-Vis spectrometry. The adsorption tests indicated a gradual decrease in the color of the MB solution. The adsorption rate begins to stabilize itself within about 120 min. In 150 min, maximum adsorption was obtained, removing about 40 % of MB coloration. The clays in natural form or after the modification process are well-known for their huge dye removal capacity (Liu and Zhang 2007). Banković et al. (2012) were able to remove 13 % of the dye tartrazine employing an iron-pillared clay, after contact for 4 h. In this work, the dye removal by the adsorption process was much higher, and a possible explanation may be the strong interaction between Fe^{3+} ions (Lewis acid) present inside and on the surface of the clay and the electron pairs of the dye structure (Song et al. 2007). In the same conditions, the montmorillonite in natural form is not able to remove a large amount of dyes, like after the iron insertion (Banković et al. 2012). Briefly, the solid surface should be modified to give higher activity, selectivity, and longer catalyst lifetime (Soon and Hameed 2011).

It is believed that most surface interactions on the clay's surface involve charge transfer reactions. The surface can acquire charge by acid–base (primary mechanism), charge transfer (ligand–donor, sorption), or ion exchange reactions (Gupta and Bhattacharyya 2012). Therefore, it is easy to understand how the presence of Fe^{3+} in the clay structure increases its dye adsorption capacity.

In the Fenton-like process (catalyst+H_2O_2), FePMAG showed a slight increase in activity for MB decoloration of about 6 % in comparison to the adsorption process (Fig. 9). This slightly higher activity in Fenton chemistry is linked to the presence of Fe^{3+} sites in the structure of the clay. The Fenton-like activity is not much higher than that because of the fact that trivalent state iron leads to a loss in the kinetics of the process (Fig. 10), since additional steps would be

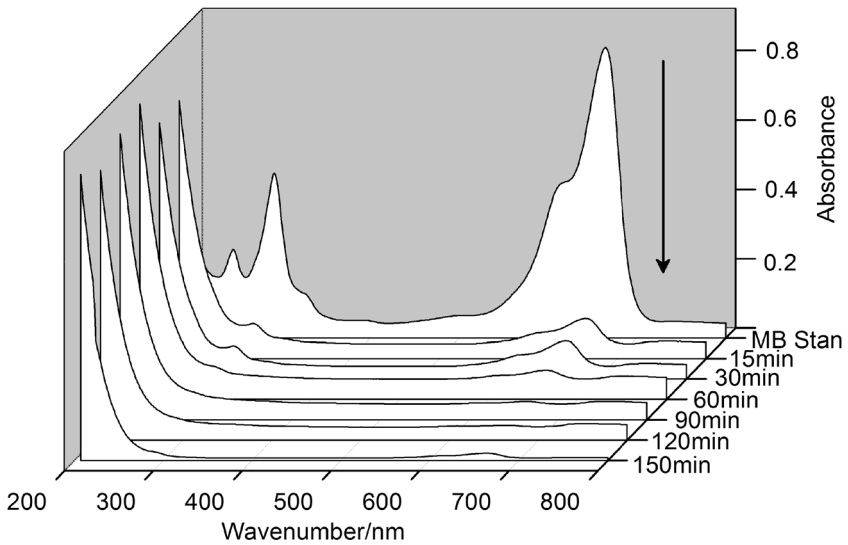

Fig. 11 Kinetic study of methylene blue oxidation with FePMAG via the photo-Fenton process (conditions: [MB]= 50 mg/L; V_{MB}=80 mL; m_{FePMAG}=30 mg; [H_2O_2]= 0.03 mol dm^{-3}; T=25±1 °C; pH=6; and λ=254 nm)

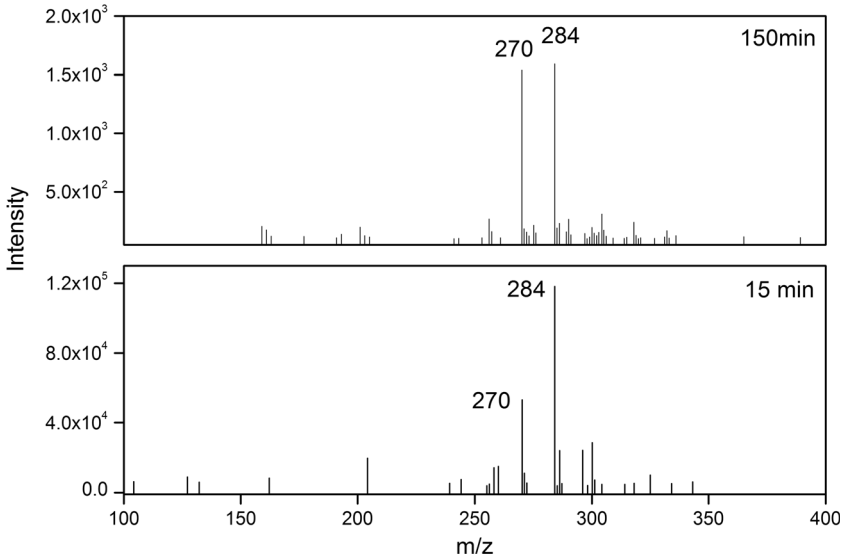

Fig. 12 Mass spectra in positive ion mode for monitoring photo-Fenton reaction at different times (initial and final time)

necessary for the initial reduction of the metal to Fe^{2+} form, as shown in Eqs. 1 and 2 (Brillas et al. 2009; Navalon et al. 2010).

$$Fe^{2+} + H_2O_2 \rightarrow Fe^{3+} + HO^- + HO^* \quad k_1 = 7.00\ \text{mol}^{-1}\text{s}^{-1} \tag{1}$$

$$Fe^{3+} + H_2O_2 \rightarrow Fe^{2+} + HOO^* + H^+ \quad k_2 = 0.001\text{–}0.01\ \text{mol}^{-1}\text{s}^{-1} \tag{2}$$

The photo-Fenton process is very similar to the Fenton-like process, except for using light (ultraviolet) concomitant to hydrogen peroxide for hydroxyl radical formation (Gogate and Pandit 2004; Pera-Titus et al. 2004). Its major efficiency is attributed to the photolysis of the ferric cations simultaneous to the Fe^{2+} and hydrogen peroxide reaction, which together form a larger amount of hydroxyl radicals (HO*). The reactions illustrating the mechanism of reactive species formation in a photo-Fenton system are shown in Eqs. 3, 4, and 5 (Herney-Ramirez et al. 2010).

$$Fe^{3+} + H_2O \rightarrow Fe(OH)^{2+} + H^+ \tag{3}$$

$$Fe(OH)^{2+} + h\nu \rightarrow Fe^{2+} + HO^* \tag{4}$$

$$Fe^{2+} + H_2O_2 \rightarrow HO^* + HO^- + Fe^{3+} \tag{5}$$

Therefore, the material FePMAG, which contains most of the maghemite phase's ferric ions (Fe^{3+}), showed a significant

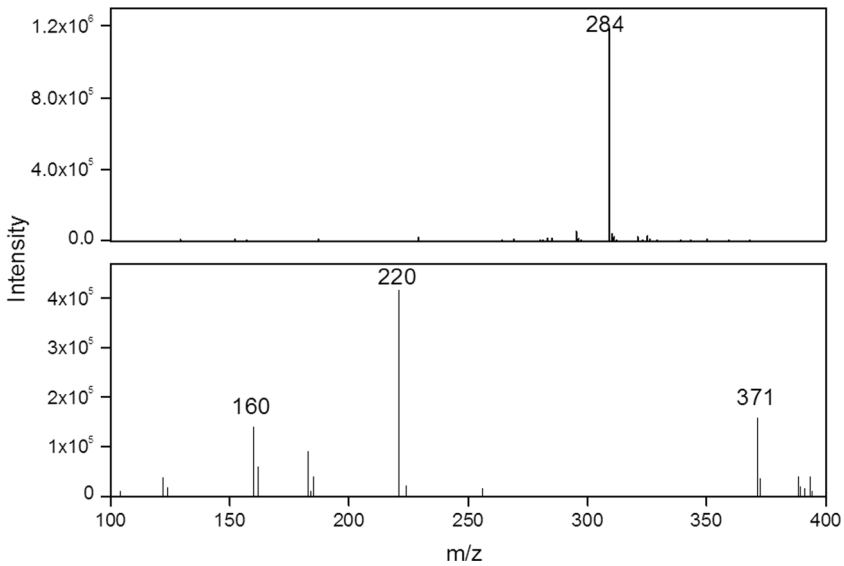

Fig. 13 Mass spectra in positive ion mode for methylene blue standard and photo-Fenton desorption product of 150 min reaction

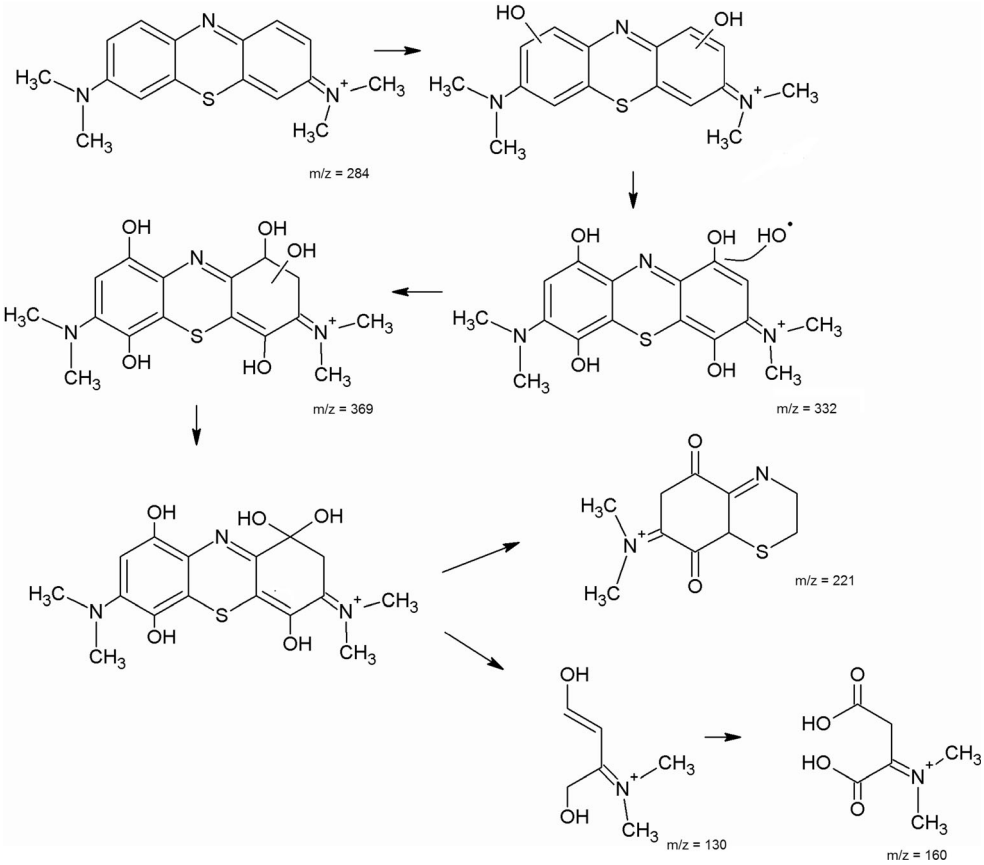

Fig. 14 Proposed scheme for the photodegradation of methylene blue molecule with FePMAG catalyst in photo-Fenton reaction (intermediate with m/z=130 and 160 proposed by Oliveira et al. 2007)

improvement when submitted to the photo-Fenton process, being able to almost completely remove the MB coloration within a short reaction time. The results of the FePMAG photo-Fenton process kinetic studies are shown in Fig. 11.

Catrinescu et al. (2012) also observed similar results, getting a huge improvement in the degradation of the molecule 4-chlorophenol by employing the photo-Fenton process (100 % for 120 min) in comparison to the Fenton-like process (100 % for 250 min), and the material used was an aluminum-pillared clay as a support to the Fe^{3+} active phase. Also, De Leon et al. (2013) found a more efficient removal percentage of methylene blue by the photo-Fenton process employing an iron-pillared clay.

The photo-Fenton results clearly show the combined effect of the catalyst, radiation, and H_2O_2 in the MB solution, with almost all of the coloration being removed after 150 min of reaction (Fig. 11). The contribution of the photocatalytic effect is remarkable at the beginning of the reaction, and it is evidenced by high degradation rates, even at short times.

Comparing the photo-Fenton and Fenton-like efficiencies, it can be said that, in the absence of radiation, hydrogen peroxide decomposition was performed on a solid surface by the complex species peroxide-Fe^{3+} active site formation. A number of reactions involving electron transfer provide the formation of Fe^{2+} active species and hydroperoxide radicals ($^{*}OOH$). The presence of radiation develops reactions which are initiated by the photoreduction of ferrous ion (Fe^{3+}) on the surface and pillars of FePMAG to ferric ion (Fe^{2+}). The Fe^{2+} on FePMAG's surface accelerates the decomposition of H_2O_2, generating HO* radicals while it is oxidized by H_2O_2 to Fe^{3+} (Fenton's reaction) (Feng et al. 2003; Herney-Ramirez et al. 2010).

Another factor that may contribute to the oxidation of methylene blue is FePMAG's great dye adsorption capacity. The adsorbed MB can be easily attacked by the hydroxyl radicals (*OH) formed in the material surface, leading to hydroxylated intermediate species or CO_2 and H_2O-like final products (Soon and Hameed 2011).

Intermediate study by mass spectrometry with electrospray ionization (ESI-MS)

The decrease in the MB solution coloration could be due to the adsorption process even if FePMAG was under radiation, if either the material does not show catalyst capacity or the iron is leaching into the solution. So, ESI-MS in positive mode was employed to identify the possible intermediate formed in methylene blue oxidation reaction.

Figure 12 presents the mass spectra obtained at the photo-Fenton reaction's initial (15 min) and final times (150 min). At

15 min, no significant reduction is observed on the m/z=384 peak relative to methylene blue and the intensity of the peak remains around 10^5. A fragment with m/z=270 appears with low intensity and has been reported by other authors as being relative to the loss of a –CH3 substituent from the amino group (Orendorz et al. 2008; Rauf et al. 2010).

At the end of the reaction, within 150 min, the MB peak (m/z=284) is significantly reduced and m/z=270 is increased, both in low intensity (10^3). No probable intermediate peaks appear, indicating no formation of MB-oxidized intermediate, as expected. However, the significant increase in MB solution decoloration during photo-Fenton associated to the complexity of FePMAG's surface and high adsorption capacity suggests the possible adsorption of oxidation products formed during the reaction.

Thus, desorption of probable reaction products from the surface of the clay was performed using acetonitrile at 35 °C for 2 h. The supernatant of this extraction was analyzed using mass spectrometry with electrospray ionization. Figure 13 shows the mass spectra obtained for the desorption product after 150 min of photo-Fenton reaction.

The mass spectrum of the desorption extraction showed several fragments relative to MB oxidation before being adsorbed by the clay's surface. The most intense peak was m/z=220, followed by m/z=371 and m/z=160. Oliveira et al. (2007), studying the MB oxidation with niobia/iron oxide composite catalyst, have already reported the peak in m/z=160 as being related to the aromatic ring cleavage after successive OH group substitutions (Fig. 14).

This study also found that the entry of successive OH groups in the MB structure causes aromatic ring cleavage simultaneous to the formation of lower molecular weight intermediates, identified by ESI-MS analysis. The oxidation products with m/z=220 and 370 had their structures suggested by this study, as well as a probable degradation path of the methylene blue molecule (Fig. 14).

Conclusions

In this work, clay with combined properties was obtained through a simple, inexpensive, and innovative route. The developed material showed magnetic properties due to the presence of maghemite iron phase, confirmed by X-ray diffraction (XRD) and X-ray photoelectron spectroscopy (XPS). This iron phase gave photoreactive activity to the montmorillonite, which was a fundamental feature for methylene blue oxidation. The pillaring process effectiveness was confirmed by XRD by an intense reflection concerning basal spacing, corresponding to an increase of around 0.57 nm compared to the starting material. The oxidation of methylene blue through the photo-Fenton process resulted in lower molecular mass molecules, identified by electrospray ionization mass spectrometry. The developed new material presents a potential for photo-Fenton degradation of contaminants in an aqueous environment.

Acknowledgments We greatly appreciate the Chemistry Departments of the Federal University of Lavras (UFLA) and São Paulo State University (UNESP), as well as this project's sponsoring organizations, National Counsel of Technological and Scientific Development (CNPQ) and Higher Education Co-ordination Agency (CAPES).

References

Afkhami A, Saber-Tehrani M, Bagheri H (2010) Modified maghemite nanoparticles as an efficient adsorbent for removing some cationic dyes from aqueous solution. Dasalination 263:240–248

Alvarez-Puebla RA, Aisa C, Blasco J, Echeverría JC, Mosquera B, Garrido JJ (2004) Copper heterogeneous nucleation on a palygorskitic clay: an XRD, EXAFS and molecular modeling study. Appl Clay Sci 25:103–110

Aronneiemi M, Lahtinen J, Hautojarvi P (2004) Characterization of iron oxide thin films. Surf Interface Anal 36:1004–1006

Ayodele OB, Lim JK, Hameed BH (2012) Pillared montmorillonite supported ferric oxalate as heterogeneous photo-Fenton catalyst for degradation of amoxicillin. Appl Catal A Gen 413–414:301–309

Banković P, Milutinović-Nikolić A, Mojović Z, Jović-Jovičić N, Žunić M, Dondur V, Jovanović D (2012) Al, Fe-pillared clays in catalytic decolorization of aqueous tartrazine solutions. Appl Clay Sci 58:73–78

Bergamini RBM, Azevedo EB, Araújo LRR (2009) Heterogeneous photocatalytic degradation of reactive dyes in aqueous TiO2 suspensions: decolorization kinetics. Chem Eng J 149:215–220

Bergaya F, Theng BKG, Lagaly G (2006) Handbook of clay science. In: Pillared clays and clays minerals. Elsevier, Amsterdam, pp 395–398

Brillas E, Sires I, Oturan MA (2009) Electro-Fenton process and related electrochemical technologies based on Fenton's reaction chemistry. Chem Rev 109:6570–6631

Cai J, Chen S, Ji M, Hu J, Ma Y, Qi L (2014) Organic additive-free synthesis of mesocrystalline hematite nanoplates via two-dimensional oriented attachment. Cryst Eng Comm 16:1553–1559

Catrinescu C, Arsene D, Apopei P, Teodosiu C (2012) Degradation of 4-chlorophenol from wastewater through heterogeneous Fenton and photo-Fenton process, catalyzed by Al–Fe PILC. Appl Clay Sci 58:96–101

Caudo S, Centi G, Genovese C, Perathoner S (2007) Copper- and iron-pillared clay catalysts for WHPCO of model and real wastewater streams from olive oil milling production. Appl Catal B Environ 70:437–446

Coelho JV, Guedes MS, Prado RG, Tronto J, Ardisson JD, Pereira MC, Oliveira LCA (2014) Effect of iron precursor on the Fenton-like activity of Fe_2O/mesoporous silica catalysts prepared under mild conditions. Appl Catal B Environ 144:792–799

Damardji B, Khalaf H, Duclaux L, David B (2009) Preparation of TiO_2-pillared montmorillonite as photocatalyst. Part I. Microwave calcination, characterization, and adsorption of a textile azo dye. Appl Clay Sci 44:201–205

De Leon MA, Sergio M, Bussi J (2013) Iron-pillared clays as catalysts for dye removal by the heterogeneous photo-Fenton technique. React Kinet Mech Cat 110:101–117

Ebner AD, Ritter JA, Navratil JD (2001) Adsorption of cesium, strontium and cobalt ions on magnetite and magnetite-silica composite. Ind Eng Chem Res 40:1615–1623

Fatimah I, Wang S, Narsito WK (2010) Composites of TiO_2-aluminum pillared montmorillonite: synthesis, characterization and photocatalytic degradation of methylene blue. Appl Clay Sci 50:588–593

Feng J, Hu X, Yue PL, Zhu HY, Lu QG (2003) A novel laponite clay-based Fe nanocomposite and its photo-catalytic activity in photo-assisted degradation of Orange II. Chem Eng Sci 58:679–685

Ferroudj N, Nzimoto J, Davidson A, Talbot D, Briot E, Dupuis V, Bée V, Medjram MS, Abramson S (2013) Maghemite nanoparticles and maghemite/silica nanocomposite microspheres as magnetic Fenton catalysts for the removal of water pollutants. Appl Catal B Environ 136–137:9–18

Galeanoa LA, Gil A, Vicente MA (2010) Effect of the atomic active metal ratio in Al/Fe-, Al/Cu- and Al/(Fe–Cu)-intercalating solutions on the physicochemical properties and catalytic activity of pillared clays in the CWPO of methyl orange. Appl Catal B Environ 100:271–281

Garrido EG, Theng BKG, Mora ML (2010) Clays and oxide minerals as catalysts and nanocatalysts in Fenton-like reactions. Appl Clay Sci 47:182–192

Gil A, Korili SA, Trujillano R, Vicente MA (2011) A review on characterization of pillared clays by specific techniques. Appl Clay Sci 53: 97–105

Gogate PR, Pandit AB (2004) A review of imperative technologies for wastewater treatment I: oxidation technologies at ambient conditions. Adv Environ Res 8:501–553

Guimarães JR, Manieiro MG, Araújo RN (2012) A comparative study on the degradation of RB-19 dye in an aqueous medium by advanced oxidation processes. J Environ Manag 110:33–39

Gupta SS, Bhattacharyya KG (2012) Adsorption of heavy metals on kaolinite and montmorillonite: a review. Phys Chem Chem Phys 14:6698–6723

Herney-Ramirez J, Vicente MA, Madeira LM (2010) Heterogeneous photo-Fenton oxidation with pillared clay-based catalysts for wastewater treatment: a review. Appl Catal B Environ 98:10–26

Homlok R, Takács E, Wojnárovits L (2013) Degradation of organic molecules in advanced oxidation processes: relation between chemical structure and degradability. Chemosphere 91:383–389

Hou MF, Ma CX, Zang WD, Tang XY, Fan YN, Wan HU (2010) Removal of rhodamine B using iron-pillared bentonite. J Hazard Mater 186:1118–1123

Jung J, Bae S, Lee W (2012) Nitrate reduction by maghemite supported Cu-Pd bimetallic catalyst. Appl Catal B Environ 127:148–158

Khalaf H, Bouras O, Perrichon V (1997) Synthesis and characterization of Al-pillared and cationic surfactant modified Algerian bentonite. Microporous Mater 8:141–150

Letaief S, Casal B, Aranda P, Martín-Luengo MA, Ruiz-Hitzky E (2003) Fe-containing pillared clays as catalysts for phenol hydroxylation. Appl Clay Sci 22:263–277

Liu P, Zhang L (2007) Adsorption of dyes from aqueous solutions or suspensions with clay nanoadsorbents. Sep Purif Technol 58:32–39

Liu XM, Fu SY, Xiao HM (2006) Synthesis of maghemite submicrospheres by simple solvothermal reduction method. J Solid State Chem 179:1554–1558

Navalon S, Alvaro M, Garcia H (2010) Heterogeneous Fenton catalysts based on clays, silicas and zeolites. Appl Catal B Environ 99:1–26

Nogueira FGE, Lopes JH, Silva AC, Gonçalves M, Anastácio AS, Sapag K, Oliveira LCA (2009) Reactive adsorption of methylene blue on montmorillonite via ESI-MS study. Appl Clay Sci 43:190–195

Oliveira LCA, Ramalho TC, Gonçalves M, Cereda F, Carvalho KT, Nazzarro MS, Sapag K (2007) Pure niobia as catalyst for the oxidation of organic contaminants: mechanism study via ESI-MS and theoretical calculations. Chem Phys Lett 446:133–137

Orendorz A, Ziegler C, Gnaser H (2008) Photocatalytic decomposition of methylene blue and 4-chlorophenol on nanocrystalline TiO_2 films under UV illumination: a ToF-SIMS study. Appl Surf Sci 255:1011–1014

Pan Z, Hua L, Qiao Y, Yang H, Zhao X, Feng B, Zhu W, Hou Z (2011) Nanostructured maghemite-supported silver catalysts for styrene epoxidation. Chin J Catal 32:428–435

Papic S, Vujevic D, Koprivanac N, Sinko D (2009) Decolourization and mineralization of commercial reactive dyes by using homogeneous and heterogeneous Fenton and UV/Fenton processes. J Hazard Mater 164:1137–1145

Pera-Titus M, Garcia-Molina V, Banos MA, Gimenez J, Espulgas S (2004) Degradation of chlorophenols by means of advanced oxidation processes: a general review. Appl Catal B Environ 47:219–256

Rauf MA, Meetani MA, Khaleel A, Ahmed A (2010) Photocatalytic degradation of methylene blue using a mixed catalyst and product analysis by LC/MS. Chem Eng J 157:373–378

Rouquerol F, Rouquerol J, Sing K (1999) Adsorption by powders and porous solids—principles, methodology and applications. Academic Press, London

Song G, Wang B, Luo H, Yang L (2007) Fe^{3+}-montmorillonite as a cost-effective and recyclable solid acidic catalyst for the synthesis of xanthenediones. Catal Commun 8:673–676

Soon AN, Hameed BH (2011) Heterogeneous catalytic treatment of synthetic dyes in aqueous media using Fenton and photo-assisted Fenton process. Desalination 269:1–16

Tuutijärvi T, Lu J, Sillanpää M, Chen G (2009) As(V) adsorption on maghemite nanoparticles. J Hazard Mater 166:1415–1420

Tyagi B, Chudasama CD, Jasra RV (2006) Determination of structural modification in acid activated montmorillonite clay by FT-IR spectroscopy. Spectrochim Acta A 64:273–278

Wang J, Wang X, Song Y, Wang J, Zhang C, Chang C, Yan J, Qiu L, Wua M, Guo Z (2013) A platinum anticancer theranostic agent with magnetic targeting potential derived from maghemite nanoparticles. Chem Sci 4:2605–2612

Yamanaka S, Doi T, Sako S, Hattori M (1984) High surface area solids obtained by intercalation of iron oxide pillars in montmorillonite. Mater Res Bull 19:161–168

Yamashita T, Hayes P (2008) Analysis of XPS spectra of Fe^{2+} and Fe^{3+} ions in oxide materials. Appl Surf Sci 254:2441–2449

Yang S, Liang G, Gu A, Mao H (2013) Synthesis of TiO_2 pillared montmorillonite with ordered interlayer mesoporous structure and high photocatalytic activity by an intra-gallery templating method. Mater Res Bull 48:3948–3954

Yu J, Yang Q-X (2010) Magnetization improvement of Fe-pillared clay with application of polyetheramine. Appl Clay Sci 48:185–190

Zhenyan P, Li H, Yunxiang Q, Hanmin Z, Xiuge Z, Bo Z, Wenwen Z, Zhenshan H (2011) Nanostructured maghemite-supported silver catalysts for styrene epoxidation. Chin J Catal 32:428–435

Zhiyong Y, Wenhua W, Lin S, Liqin L, Zhiyin W, Xuanfeng W, Chaonan D, Ruiying Q (2013) Acceleration comparison between Fe^{2+}/H_2O_2 and Co^{2+}/oxone for decolouration of azo dyes in homogeneous systems. Chem Eng J 234:475–483